Molecular Plant • Volume 5 • Number 6 • Pages 1281–1294 • November 2012 RESEARCH ARTICLE

DICER-LIKE3 Activity in *Physcomitrella patens DICER-LIKE4* Mutants Causes Severe Developmental Dysfunction and Sterility

M. Asif Arif[a], Isam Fattash[a], Zhaorong Ma[b], Sung Hyun Cho[b], Anna K. Beike[a], Ralf Reski[a,c,d,e], Michael J. Axtell[b] and Wolfgang Frank[a,c,1]

a Plant Biotechnology, Faculty of Biology, University of Freiburg, Schaenzlestraβe 1, D-79104 Freiburg, Germany
b Department of Biology, Pennsylvania State University, University Park, PA 16802, USA
c FRISYS Freiburg Initiative for Systems Biology, D-79104 Freiburg, Germany
d BIOSS Centre for Biological Signalling Studies, D-79104 Freiburg, Germany
e FRIAS Freiburg Institute for Advanced Studies, D-79104 Freiburg, Germany

ABSTRACT ***Trans*-acting small interfering RNAs (ta-siRNAs) are plant-specific siRNAs released from *TAS* precursor transcripts after microRNA-dependent cleavage, conversion into double-stranded RNA, and Dicer-dependent phased processing. Like microRNAs (miRNAs), ta-siRNAs direct site-specific cleavage of target RNAs at sites of extensive complementarity. Here, we show that the DICER-LIKE 4 protein of *Physcomitrella patens* (PpDCL4) is essential for the biogenesis of 21 nucleotide (nt) ta-siRNAs. In Δ*PpDCL4* mutants, off-sized 23 and 24-nt ta-siRNAs accumulated as the result of PpDCL3 activity. Δ*PpDCL4* mutants display severe abnormalities throughout *Physcomitrella* development, including sterility, that were fully reversed in Δ*PpDCL3*/Δ*PpDCL4* double-mutant plants. Therefore, PpDCL3 activity, not loss of PpDCL4 function per se, is the cause of the Δ*PpDCL4* phenotypes. Additionally, we describe several new *Physcomitrella trans*-acting siRNA loci, three of which belong to a new family, *TAS6*. *TAS6* loci are typified by sliced miR156 and miR529 target sites and are in close proximity to *PpTAS3* loci.**

Key words: ta-siRNA; miR156; PpDCL3; PpDCL4; development; moss.

INTRODUCTION

In plants, different RNA silencing pathways regulate gene expression during development (Du and Zamore, 2005), control genome maintenance (Xie et al., 2004), and act in defense against biotic and abiotic stresses (Borsani et al., 2005; Deleris et al., 2006). For the regulation of these diverse processes, plants evolved complex small non-coding RNA (sRNA) pathways consisting of miRNA, ta-siRNA, natural antisense transcript-derived small interfering RNA (nat-siRNA), and repeat-associated small interfering RNA (ra-siRNA) (Vazquez, 2006). Most plant species possess a set of four Dicer proteins (Margis et al., 2006) with specific functions in the biogenesis of sRNAs from double-stranded RNA precursors. In *Arabidopsis thaliana*, DCL1 is required for the maturation of miRNAs from hairpin precursors (Park et al., 2002; Reinhart et al., 2002), DCL2 acts in the generation of siRNAs from exogenous RNA sources (Xie et al., 2004), DCL3 guides siRNA formation from heterochromatin-associated regions (Herr et al., 2005; Xie et al., 2004), and DCL4 acts in the formation of ta-siRNAs (Dunoyer et al., 2005; Xie et al., 2005). Although each Dicer protein is associated with a specific pathway, functional redundancies between the individual Dicers do exist (Gasciolli et al., 2005; Henderson et al., 2006; Fahlgren et al., 2009). The *Physcomitrella* genome also encodes four DCL proteins, but the DCL repertoire varies from that in the flowering plant *Arabidopsis*. Two *Physcomitrella* homologs, PpDCL1a and PpDCL1b, show high similarity to AtDCL1, PpDCL3 and PpDCL4 proteins are homologous to AtDCL3 and AtDCL4, respectively, whereas an AtDCL2 ortholog is missing (Axtell et al., 2007). PpDCL1a is essential for miRNA biogenesis and thus the functional equivalent to AtDCL1 whereas PpDCL1b is required for miRNA-directed cleavage of target RNAs (Khraiwesh et al., 2010). Unlike *Arabidopsis* DCL3, which produces exclusively 24-nt siRNAs (Xie et al., 2004; Gasciolli et al., 2005), *PpDCL3* is required for the accumulation of

[1] To whom correspondence should be addressed. E-mail wolfgang.frank@biologie.uni-freiburg.de, tel. +49 761 203 2820, fax +49 761 203 6945.

doi:10.1093/mp/sss036, Advance Access publication 17 April 2012
Received 27 October 2011; accepted 27 February 2012

22–24-nt siRNAs (Cho et al., 2008). In both species, DCL3-dependent siRNAs arise preferentially from intergenic and repetitive genomic regions with dense cytosine methylation (Kasschau et al., 2007; Cho et al., 2008). Moreover, Δ*PpDCL3* mutants display accelerated gametophore development, while *Arabidopsis dcl3* mutants show no obvious developmental defects. *Arabidopsis dcl2*/*dcl3* or *dcl3*/*dcl4* double mutants show stochastic developmental defects that are more severe in *dcl2*/*dcl3*/*dcl4* triple mutants, suggesting functional redundancy between these proteins (Gasciolli et al., 2005; Cho et al., 2008).

miRNAs and ta-siRNAs act by base-pairing to their target RNAs, thereby mediating cleavage or translational repression of the target (Qi and Hannon, 2005). Both miRNAs and ta-siRNAs are ~21 nt in size and are nuclear-encoded, but they differ with respect to their biogenesis from RNA precursors (Vaucheret, 2006). Primary *MIRNA* transcripts have a characteristic stem-loop structure that is processed into mature miRNA. *TAS* precursor transcripts contain miRNA binding sites leading to miRNA-directed precursor cleavage, subsequent conversion of the cleavage products into dsRNA by RNA-DEPENDENT RNA POLYMERASE (RDR), and phased dicing of the dsRNA into ta-siRNAs by Dicer proteins (Allen et al., 2005; Talmor-Neiman et al., 2006).

In *Arabidopsis*, several components of the ta-siRNA biogenesis pathway were identified, including three miRNAs (miR173, miR390, and miR828) that direct site-specific cleavage of distinct *TAS* transcripts, RDR6 catalyzing the conversion into dsRNA, SUPPRESSOR OF GENE SILENCING 3 (SGS3) protecting the *TAS* precursors from degradation, ARGONAUTE 1/7 (AGO1/7) for miRNA-directed cleavage of *TAS* precursors, DICER-LIKE4 (DCL4) for the phased slicing of double-stranded *TAS* precursors, and DOUBLE-STRANDED RNA BINDING PROTEIN 4 (DRB4) that interacts with DCL4 for proper dicing activity (Peragine et al., 2004; Vazquez et al., 2004; Allen et al., 2005; Gasciolli et al., 2005; Xie et al., 2005; Yoshikawa et al., 2005; Adenot et al., 2006).

In *Arabidopsis*, four *TAS* gene families (*TAS1–4*) have been identified. Ta-siRNA production from *TAS1* and *TAS2* requires miR173-directed cleavage, miR390 is dedicated to *TAS3*, and miR828 is assigned for *TAS4* (Allen et al., 2005; Rajagopalan et al., 2006). In *Arabidopsis*, most miRNAs are incorporated into an AGO1-containing RNA-induced silencing complex (RISC) to direct cleavage of their targets, whereas miR390-dependent cleavage of *TAS3* requires AGO7 activity (Montgomery et al., 2008). In *Physcomitrella*, ta-siRNAs originate from four *TAS3* precursors (*TAS3a–d*) that possess miR390-dependent cleavage at two distinct sites spanning the region from which ta-siRNAs are produced (Axtell et al., 2006; Talmor-Neiman et al., 2006). Recently, a fifth *TAS* family (*TAS5*) was identified in tomato; sly-*TAS5* is triggered by miR482-directed slicing (Li et al., 2012).

Physcomitrella ta-siRNAs regulate transcription factor transcripts encoding a single N-terminal AP2 domain and, similarly to *Arabidopsis*, mRNAs encoding ARF (Auxin Response Factor) transcription factors (Talmor-Neiman et al., 2006; Axtell et al., 2007). However, to date, a functional analysis of the DCL protein acting in the biogenesis of *Physcomitrella* ta-siRNAs is missing. The only study on *Physcomitrella* ta-siRNA biogenesis revealed an essential function of *PpRDR6* that is required for the accumulation of ta-siRNAs. Δ*PpRDR6* mutant lines lack ta-siRNAs and display an accelerated developmental transition from the juvenile (protonema) to the adult gametophyte (gametophore) (Talmor-Neiman et al., 2006).

Here, we demonstrate that Δ*PpDCL4* loss-of-function mutants have dramatic developmental abnormalities. In the Δ*PpDCL4* background, PpDCL3 processes *TAS* substrates into 'off-sized' 23–24-nt siRNAs. The Δ*PpDCL4* developmental defects are fully ameliorated in Δ*PpDCL3*/Δ*PpDCL4* double mutants, which completely lack *TAS*-derived sRNAs of all sizes. Therefore, an activity of *PpDCL3*, not the reduced effectiveness of ta-siRNA function, is responsible for the Δ*PpDCL4* developmental phenotypes. We also identified a new family of *TAS* loci, *PpTAS6*, characterized by dual miR156 and/or miR529-mediated cleavage sites and close genomic proximity to *PpTAS3* loci.

RESULTS

Loss of *PpDCL4* Results in Severe Developmental Abnormalities

The functional characterization of the *PpDCL4* gene was initiated by cloning and sequencing of its full-length cDNA, revealing that it contains all characteristic domains of Dicer proteins (Supplemental Figure 1A). *Physcomitrella* integrates DNA into its nuclear genome by means of homologous recombination at high frequencies (Strepp et al., 1998) enabling the targeted disruption of genomic loci. Making use of the efficient gene targeting, we generated four independent *PpDCL4* null mutants (Δ*PpDCL4*) by the insertion of a *zeocin* selection marker cassette into the *PpDCL4* genomic locus (Supplemental Figure 1B–1D). Two independent Δ*PpDCL4* mutant lines that have integrated a single copy of the *PpDCL4* gene disruption construct at the *PpDCL4* genomic locus (Supplemental Figure 1E) were used for further analyses.

In *Arabidopsis dcl4* mutants, the lack of ta-siRNAs only has minor developmental effects, namely the formation of downward curled and slightly elongated rosette leaf margins and accelerated juvenile-to-adult vegetative phase changes (Gasciolli et al., 2005; Xie et al., 2005). In contrast, *Oryza sativa dcl4* mutants display developmental defects in the leaves, are semi-dwarfed, display a severe disturbance of spikelet organ identity, and are sterile (Liu et al., 2007). Comparable to rice *dcl4* mutants, we observed severe developmental defects throughout the development of Δ*PpDCL4* mutants. Under long-day conditions, Δ*PpDCL4* mutants display an aberrant colony morphology characterized by a reduced size and a strongly increased development of filamentous protonema tissue (Figure 1A). *Physcomitrella* protonema tissue comprises two cell types: chloronema and caulonema cells. Chloronema

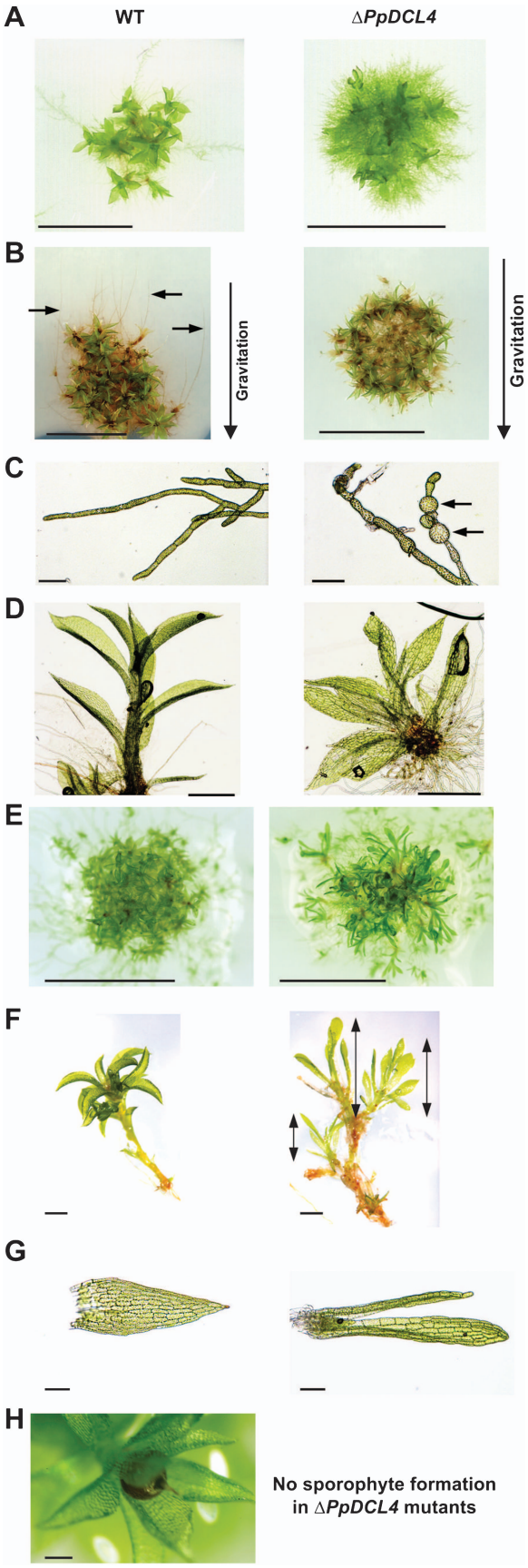

cells are short, chloroplast-enriched, and characterized by cross walls that are perpendicular to the growth axis. Caulonema cells are elongated and thinner, they contain fewer chloroplasts, and their cross walls are oblique to the growth axis (Reski, 1998). Caulonema development can be triggered by growth in the dark (Vandenbussche et al., 2007). Wild-type plants cultivated for 8 d in complete darkness developed numerous caulonema filaments with a negative gravitropic growth response whereas dark-induced caulonema formation was abolished in the Δ*PpDCL4* mutant lines (Figure 1B).

Under various stress conditions or in response to ABA treatment, subapical chloronema cells can form short, thick-walled, rounded brood-cells called brachycytes (Schnepf and Reinhard, 1997; Decker et al., 2006) that act as vegetative spores to ensure plant survival under unfavorable growth conditions. In contrast to the wild-type, Δ*PpDCL4* mutants developed a high number of brachycytes even under standard growth conditions (Figure 1C). Further development of protonema tissue is characterized by the formation of three-faced apical cells (buds) that give rise to the leafy gametophores. Δ*PpDCL4* mutants are also affected in gametophore development, since gametophores are dwarfed under long- and short-day conditions (Figure 1D and 1F). Furthermore, when grown under short-day conditions, the leaf shape of Δ*PpDCL4* mutants deviates severely from wild-type characterized by the development of spatulate elongated leaves with serrate leaf margins (Figure 1E–1G).

Most strikingly, in the Δ*PpDCL4* mutant lines, sexual reproduction is abolished, since they are not able to develop the diploid sporophyte. At low temperatures and under inductive conditions, male (antheridia) and female (archegonia) sex organs are formed at the apices of gametophores (Hohe

Figure 1. Phenotypic Analyses of Δ*PpDCL4* Mutants.
Both independent Δ*PpDCL4* mutants display an identical mutant phenotype. Representative images of one line are shown.
(A) Equal amounts of protonema tissue from wild-type (WT) and the Δ*PpDCL4* mutant were spotted onto solid medium and grown under long-day conditions. Colonies were photographed after 4 weeks. Note the increased protonema development in the Δ*PpDCL4* mutant. Scale bar: 0.5 cm.
(B) Cultivation for 8 d in darkness results in caulonema formation in WT (black arrows), but not in the Δ*PpDCL4* mutant. Scale bar: 0.5 cm.
(C) The Δ*PpDCL4* mutant develops a high number of brachycytes (arrows). Scale bar: 0.1 mm.
(D) Under long-day growth conditions, the Δ*PpDCL4* mutant develops dwarfed gametophores. Scale bar: 1 mm.
(E) As in (A) grown under short-day conditions. Scale bar: 1 cm.
(F) The gametophores of the Δ*PpDCL4* mutant are dwarfed when grown under sporophyte-inducing short-day conditions. Gametophore size in the Δ*PpDCL4* mutant is indicated by arrows. Scale bar: 1 mm.
(G) The Δ*PpDCL4* mutant develops abnormal spathulate elongated leaves. Scale bar: 0.1 mm.
(H) The Δ*PpDCL4* mutant fails to develop sporophytes. Scale bar: 200 μm.

et al., 2002). In the presence of water, spermatozoids reach the archegonia and fertilize the egg cell. After fertilization, the diploid sporophyte develops and, after meiosis, haploid spores are formed within the spore capsule. When wild-type plants were grown under sporophyte-inducing conditions, all 27 analyzed colonies developed maturing sporophytes (Figure 1H). In contrast, sporophyte development was completely abolished in the Δ*PpDCL4* mutant lines (27 colonies analyzed from each Δ*PpDCL4* mutant line). As the defect in sporophyte development in the Δ*PpDCL4* mutants might be caused by defective male and/or female reproductive tissues, we analyzed the morphology of antheridia and archegonia, but did not observe morphological deviations. Consequently, a cross-fertilization experiment was performed with Δ*PpDCL4* mutants and *Physcomitrella* wild-type. To investigate whether the defective sporophyte formation in the Δ*PpDCL4* mutants is caused by female sterility, we co-cultivated Δ*PpDCL4* mutant lines with wild-type colonies and induced sporophyte formation. In case of male sterility, defects in spermatozoid development in the mutant lines should be complemented by wild-type spermatozoids and should result in the fertilization of egg cells in the archegonia of Δ*PpDCL4* mutants. If the development of the female reproductive tissue is affected in the mutant lines, fertilization cannot be compensated by wild-type spermatozoids. Since only wild-type colonies formed sporophytes on mixed plates, but the mutant plants did not, we infer that at least the development of female reproductive tissues is affected in Δ*PpDCL4* mutants. However, in addition to that, we cannot exclude defective spermatozoid development in the Δ*PpDCL4* mutants as well.

PpDCL4 Is Required for Normal ta-siRNA Accumulation and Function

In order to obtain a genome-wide view on *PpDCL4* functions in *Physcomitrella* sRNA pathways, we compared sRNA profiles from protonema tissue of Δ*PpDCL4* mutants and wild-type by smallRNAseq, a commonly used quantitative sRNA profiling method (Lu et al., 2006; Ruby et al., 2006; Kasschau et al., 2007; Lister et al., 2008). Size-fractionated small RNAs (~10–40 nt) from wild-type and Δ*PpDCL4* mutant line 1 harboring a single genomic integration of the Δ*PpDCL4* knockout construct at the *PpDCL4* locus were sequenced using the SOLiD™ 2 system (Applied Biosystems). Subsequent analysis was restricted to reads with a length of 20–24 nt, resulting in 32 467 reads from wild-type and 106 609 reads from the Δ*PpDCL4* mutant. The data were normalized as reads per 10 000 and used to analyze sRNA expression and size distribution from previously described *MIR* and *TAS* loci.

In *Arabidopsis*, DCL1 is the essential enzyme for the processing of miRNAs from hairpin-like *MIR* precursor transcripts (Park et al., 2002; Reinhart et al., 2002), whereas the *Arabidopsis* DCL4 protein has no effect on miRNA biogenesis (Xie et al., 2005) with the exception of a few irregular, non-conserved miRNAs (Rajagopalan et al., 2006). We observed similar results in *Physcomitrella*: no apparent differences were observed in the overall accumulation and size distribution of miRNAs between *Physcomitrella* wild-type and Δ*PpDCL4* (Figure 2A and Supplemental Table 1). RNA blots of select miRNAs confirmed that Δ*PpDCL4* mutants did not substantially affect miRNA accumulation (Figure 2B). These results are in agreement with our previous studies that identified PpDCL1a to be the essential protein for the maturation of miRNAs in *Physcomitrella* (Khraiwesh et al., 2010).

The Δ*PpDCL4* mutants are strongly affected in the accumulation of *TAS3*-derived ta-siRNAs. Overall, ta-siRNA accumulation was strongly reduced, and the remaining ta-siRNAs were shifted in size from the wild-type 21–22-nt-dominated profile to a 23–24-nt-dominated profile in the mutant (Figures 2C and 2D). The off-sized ta-siRNAs observed in the Δ*PpDCL4* mutant still appeared to be in phase with the flanking miR390 cleavage sites (Supplemental Figure 2), suggesting that an alternative PpDCL protein substituted for PpDCL4 at the *TAS3* loci in the Δ*PpDCL4* plants. Two known targets of *PpTAS3*-derived ta-siRNAs accumulated to higher levels in the Δ*PpDCL4* mutant, suggesting that ta-siRNA target regulation was compromised in the Δ*PpDCL4* background (Figure 2E). One of the two targets analyzed, the *Auxin Response Factor* (*ARF*) transcript *Phypa_203442*, was previously shown to be targeted by both a miRNA (miR1219) and a *PpTAS3*-derived ta-siRNA, which we refer to as ta-siARF (Axtell et al., 2007). 5′-RACE experiments demonstrated that, while miR1219-mediated cleavage of this *ARF* transcript persisted in the Δ*PpDCL4* mutant, ta-siARF-mediated cleavage was not detectable (Figure 2F).

PpDCL3 Is Responsible for the Phenotypes of Δ*PpDCL4* Mutants

PpDCL3 is required for the accumulation of repeat-associated 22–24-nt siRNAs that derive from densely methylated, intergenic regions of the *Physcomitrella* genome (Cho et al., 2008). Because the off-sized ta-siRNAs that accumulate in the Δ*PpDCL4* mutants are also dominated by 22–24-nt-long species, we hypothesized that, in the absence of PpDCL4, PpDCL3 processes *TAS3* dsRNAs, and that the resulting siRNAs are funneled into the PpDCL3-dependent siRNA pathway, perhaps directing inappropriate chromatin modifications at siRNA-generating loci. Consistently with this notion, the accumulation of *PpTAS3a* primary transcripts was reduced in Δ*PpDCL4* mutants (Figure 3A). From bisulfite-treated DNA cytosine methylation-specific primers only amplified *PpTAS3*-derived PCR products from the Δ*PpDCL4* mutant lines, whereas primers specific for non-methylated sequences exclusively generated PCR products from wild-type (Figure 3B). Subsequent cloning and sequencing of the PCR products revealed that *PpTAS3a* residues were highly methylated in the Δ*PpDCL4* mutants (Supplemental Figure 3). We detected cytosine methylation in both symmetrical (CG and CHG) and non-symmetrical (CHH) DNA sequence contexts. Since cytosine methylation of nuclear DNA is well known to cause epigenetic transcriptional silencing (Chan et al., 2005; Goll and Bestor, 2005), we propose that the high degree of cytosine methylation in the *PpTAS3a*

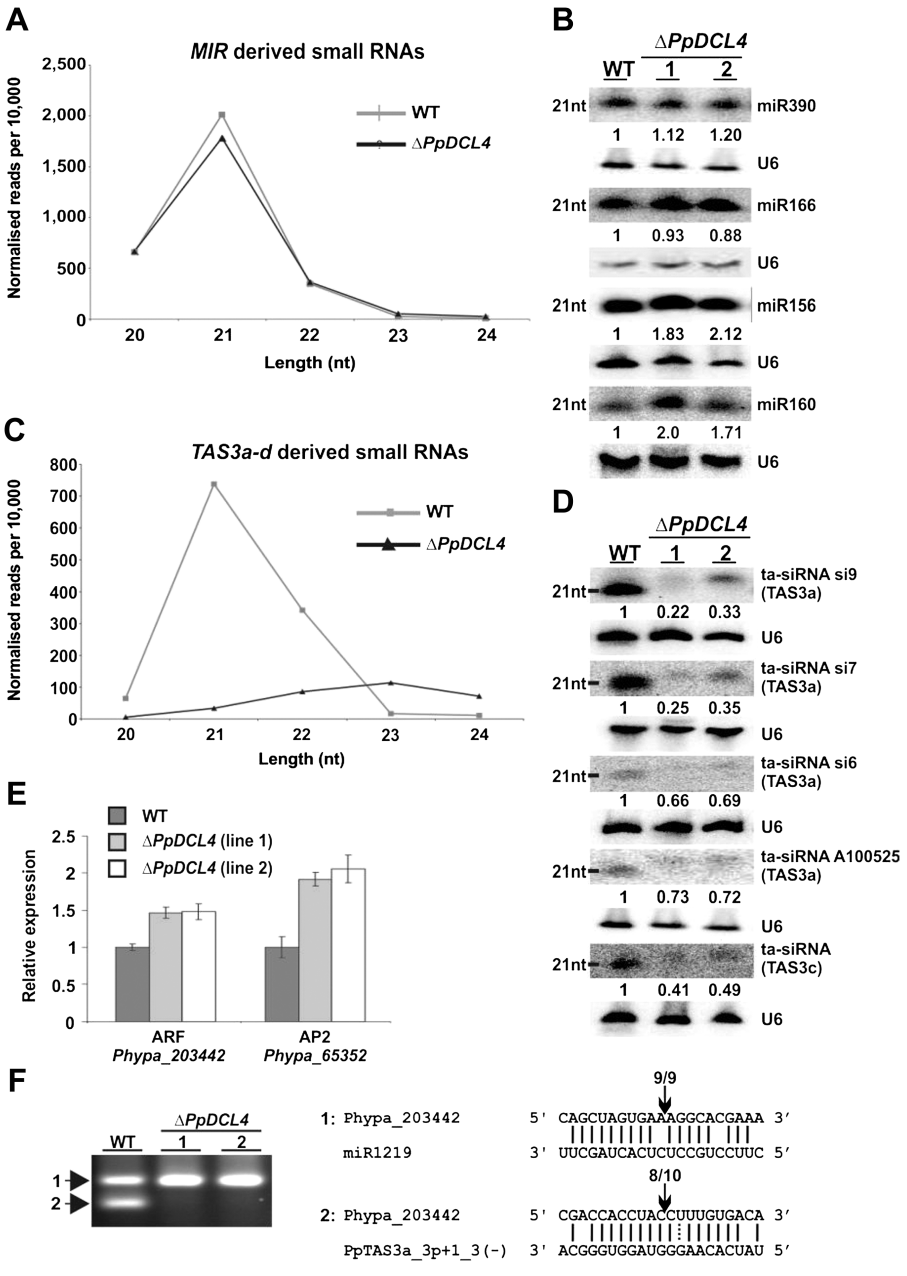

Figure 2. Analyses of miRNAs and ta-siRNAs in Δ*PpDCL4* Mutants.
(A) Summed, scaled, repeat-normalized sRNA abundances for all *MIRNA*-derived sRNAs from wild-type and Δ*PpDCL4*. Units are normalized reads per 10 000.
(B) Expression analysis of miR390, miR166, miR156, and miR160 in protonema tissue by RNA gel blots. U6 snRNA served as control for normalization. Numbers under blots indicate normalized expression values with respect to wild-type.
(C) Chart indicating the expression of *TAS3a-d* derived sRNAs inferred from sequencing data of wild-type and Δ*PpDCL4*.
(D) RNA gel blots for ta-siRNAs derived from *TAS3a* and *TAS3c* precursors in wild-type and Δ*PpDCL4* mutants. U6snRNA served as control for normalization. Numbers under blots indicate normalized expression values for off-sized ta-siRNAs with respect to the 21-nt wild-type ta-siRNAs.
(E) Transcript levels of ta-siRNA target genes (*PpARF; Phypa_203442* and *PpAP2; Phypa_65352*) in wild-type (WT) and Δ*PpDCL4* mutants determined by qRT–PCR. Expression levels were normalized to the constitutively expressed control gene *PpEF1α*.
(F) RLM 5′ RACE products of the miRNA and ta-siRNA target *PpARF* from WT and Δ*PpDCL4* mutants. Arrows mark products of the expected size (1: miRNA-mediated cleavage product; 2: ta-siRNA-mediated cleavage product) that were eluted, cloned, and sequenced. Numbers above miRNA:target and ta-siRNA:target alignments indicate sequenced RACE products with the corresponding 5′ end.

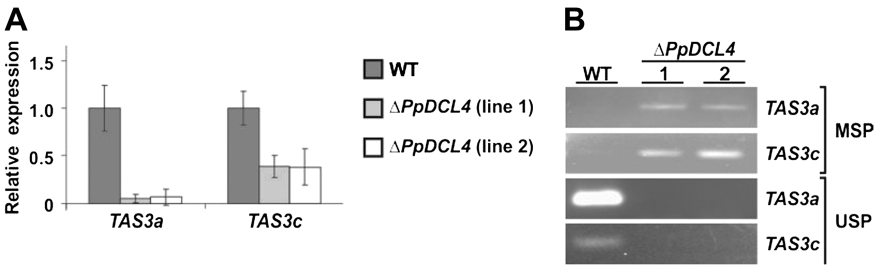

Figure 3. Reduced Transcript Accumulation and Increased DNA Methylation at *TAS* Loci in Δ*PpDCL4* Mutants.
(A) Expression level of the *TAS* precursors *TAS3a* and *TAS3c* determined by qRT–PCR. Expression levels were normalized to the constitutively expressed control gene *PpEF1α*.
(B) Bisulfite PCR with methylation-specific (MSP) and unmethylation-specific (USP) primers for *TAS3a* and *TAS3c*.

loci of Δ*PpDCL4* mutants is directed by *PpDCL3*-dependent siRNAs and leads to reduced *PpTAS3a* transcription rates. However, it is important to note that the ectopic DNA methylation of *PpTAS3a* and associated reduction of the *PpTAS3a* primary transcript are unlikely to cause the developmental phenotypes observed in Δ*PpDCL4*, as complete absence of ta-siRNAs in the Δ*PpRDR6* mutant does not cause a similar phenotype. To prove this hypothesis, we generated Δ*PpDCL3*/Δ*PpDCL4* double mutants by first establishing a Δ*PpDCL3* mutant line that integrated a single *PpDCL3* knockout construct at the *PpDCL3* locus and was confirmed to be a null mutant by RT–PCR (Supplemental Figure 4A–4E). Subsequently, the *PpDCL4* knockout construct was introduced into the Δ*PpDCL3* mutant background resulting in the generation of six independent Δ*PpDCL3*/Δ*PpDCL4* double mutants, all of which were confirmed to lack both the *PpDCL3* and *PpDCL4* transcripts (Supplemental Figure 4F). Strikingly, the developmental defects observed in the Δ*PpDCL4* mutants were not present in the Δ*PpDCL3*/Δ*PpDCL4* double mutants (Figures 4A–4D). The colony morphology, protonema shape, size of gametophores, caulonema initiation in the dark, gametangia development, sporophyte formation, and maturation of spore capsules in Δ*PpDCL3*/Δ*PpDCL4* mutants were similar to wild-type. In Δ*PpDCL3*/Δ*PpDCL4* mutants, we only observed an accelerated gametophore production that resembles the phenotype of Δ*PpDCL3* mutants (Cho et al., 2008) as well as the Δ*PpRDR6* mutants (Talmor-Neiman et al., 2006). RNA blots indicated that ta-siRNAs of all sizes were completely absent in Δ*PpDCL3*/Δ*PpDCL4* mutants, while miRNA accumulation was unaffected (Figure 4E). We therefore conclude that the developmental defects caused by loss of *PpDCL4* function cannot be attributed solely to reduction of ta-siRNA accumulation. Instead, the *PpDCL4* phenotypes are caused by *PpDCL3* activity, which only manifests in the absence of *PpDCL4* function. We further characterized the PpDCL3-dependent ta-siRNAs by performing target prediction with the 23 and 24-nt *PpTAS3a*-derived small RNAs present in the Δ*PpDCL4* small RNA library. With maximum stringent conditions of target prediction, we identified 69 target sites from 49 distinct genes that are probably affected in the Δ*PpDCL4* mutant (Supplemental Table 2).

Identification of Additional *DCL4/RDR6*-Dependent *TAS* Loci in *Physcomitrella*

The four previously known *PpTAS3* loci were discovered based upon phased patterns of siRNA accumulation and the presence of miR390 complementary sites (Axtell et al., 2006; Talmor-Neiman et al., 2006). As described above, siRNA accumulation patterns at these four loci change in distinctive patterns in Δ*PpDCL4* and Δ*PpRDR6* plants; Δ*PpDCL4* mutants shift the size profile of the siRNAs from a 21-nt-dominated pattern to a 23–24-nt-dominated pattern, while nearly all siRNA accumulation is lost in Δ*PpRDR6* mutants. We therefore used existing *Physcomitrella* smallRNAseq data to search for additional small RNA loci showing similar changes in siRNA accumulation in Δ*PpDCL4* and Δ*PpRDR6* plants. Initially, seven loci were identified, four of which overlapped the previously described *PpTAS3a-d* (Figure 5, Table 1, and Supplemental Figure 5). Two of the three novel loci overlapped previously described hotspots of non-miRNA 21nt-dominated small RNA expression (*Pp21SR6* and *Pp21SR39*; Cho et al., 2008). The third novel locus as well as *Pp21SR6* possessed dual miR390 complementary regions and thus we named them *PpTAS3e* and *PpTAS3f*, respectively. Degradome data (Addo-Quaye et al., 2009) demonstrated that the four miR390 sites within *PpTAS3e* and *PpTAS3f* were sliced (Table 1 and Supplemental Figure 5). Two distinct *PpTAS3* ta-siRNA populations have previously been shown to be capable of directing the slicing of targets *in trans*: one population targets *AP2*-domain transcripts, while the other directs slicing of *ARF*-domain transcript (Talmor-Neiman et al., 2006; Axtell et al., 2007; Khraiwesh et al., 2010). *PpTAS3e* could produce a ta-siARF with reasonable base-pairing to one of the known ta-siARF target sites, while *PpTAS3f* could produce both ta-siAP2 and ta-siARF (Table 1, Supplemental Figure 5, and Supplemental Table 3). The *PpTAS3e* siRNA population was typical in that it was largely contained between, and in phase with, the two miR390 complementary regions (Supplemental Figure 5). In contrast, the *PpTAS3f* siRNA population extended beyond the region bounded by the dual miR390 complementary sites, and was not well phased (Supplemental Figure 5).

The final novel *DCL4*/*RDR6*-dependent siRNA locus that we found in our initial computational screen produced siRNAs from a region bounded by upstream miR156 and miR529 complementary sites and a downstream miR156 site (Figure 5A). Degradome data support slicing at all three complementary sites and the siRNA population is largely in a 21-nt phase with the 3′ miR156 cleavage site (Figure 5A). This locus, previously described as *Pp21SR39* but heretofore unrecognized as a *TAS* locus (Cho et al., 2008), did not share detectable similarity with any previously described families of plant *TAS* loci. Therefore, we renamed it *PpTAS6a*. Curiously, *PpTAS6a* is located within ~0.7 kb of *PpTAS3a*, and their respective miRNA complementary sites are located on the same strand (Figure 5A). Inspection of the genomic region surrounding *PpTAS3f* revealed a second nearby cluster of mainly 21-nt siRNAs in the wild-type. We found that this region also contained a high-confidence miR156 complementary site downstream of the siRNA-generating region, which showed degradome-based evidence of slicing (Supplemental Figure 5). In addition, upstream miR156 and miR529 sites could also be observed, albeit with extensive mismatches and no evidence of slicing. Based on this fact, we named this locus *PpTAS6b*, although there was no detectable sequence similarity outside of the pattern of miR156 and miR529 complementary sites between *PpTAS6a* and *PpTAS6b*. Like its neighbor *PpTAS3f*, siRNA production from *PpTAS6b* was atypical in that it was not in phase with the miRNA-directed cleavage site(s) and extended for a long distance beyond the complementary sites (Supplemental Figure 5). Finally, we detected sequence similarity between *PpTAS6a* and a region neighboring *PpTAS3d*. Although we could find no evidence of small RNA production from this region, we did observe a pattern of miR156 and

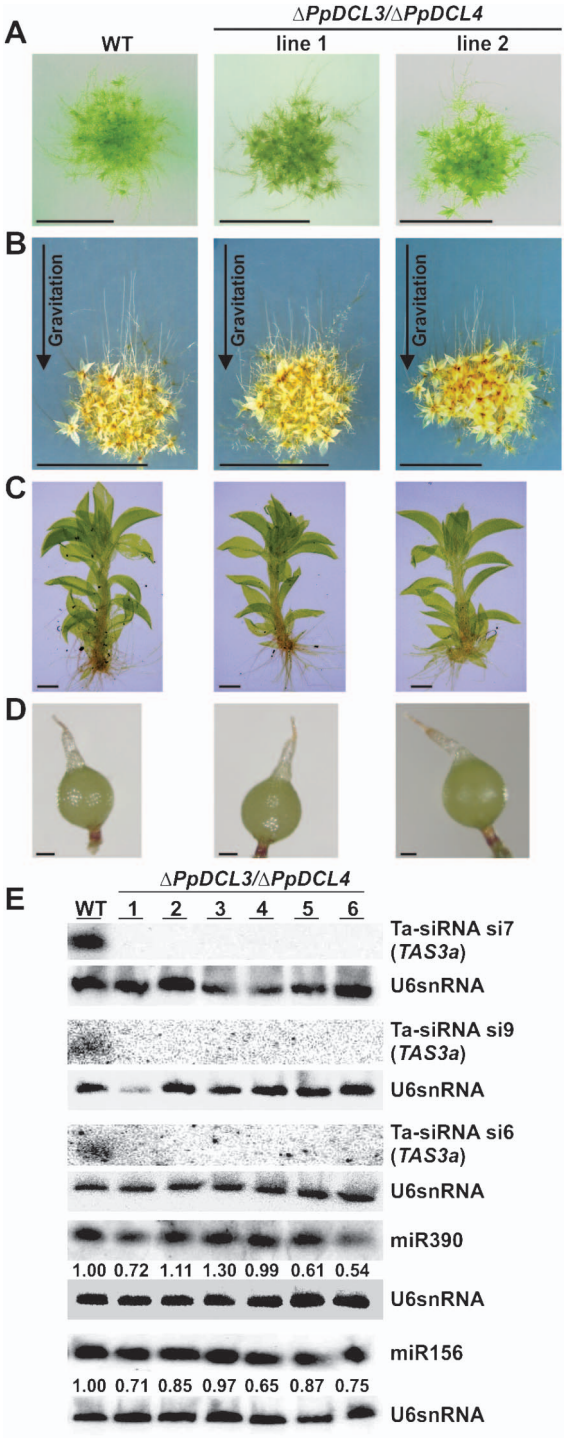

Figure 4. Phenotypic Analyses of Δ*PpDCL3*/Δ*PpDCL4* Double Mutants.

(A) Equal amounts of protonema tissue from wild-type (WT) and Δ*PpDCL3*/Δ*PpDCL4* mutants were spotted onto solid medium and developed colonies were photographed after 3 weeks. Δ*PpDCL3*/Δ*PpDCL4* mutants show accelerated gametophore development. Scale bar: 0.5 cm.

(B) WT and Δ*PpDCL3*/Δ*PpDCL4* mutants display normal caulonema development after 10 d growth in darkness. Scale bar: 0.5 cm.

(C) Gametophore size is similar in WT and Δ*PpDCL3*/Δ*PpDCL4* mutants. Scale bar: 2 mm.

(D) Sporophyte formation is rescued in Δ*PpDCL3*/Δ*PpDCL4* mutants. Scale bar: 200 μm.

(E) RNA gel blots hybridized with antisense probes of miR390, miR156, and ta-siRNAs generated from the *PpTAS3a* precursor in WT and Δ*PpDCL3*/Δ*PpDCL4* double mutants. An antisense probe for U6 snRNA served as control for normalization. Numbers under blots indicate normalized miRNA expression values with respect to WT.

miR529 complementary sites similar to the other *TAS6* loci with some weak evidence of slicing; therefore, we have provisionally named this locus *PpTAS6c* (Supplemental Figure 5). Phylogenetic analysis demonstrated that the six *PpTAS3* loci fall into two distinct clades: *PpTAS3a*, *-d*, and *-f* form one clade, while *PpTAS3b*, *-c*, and *-e* form the other clade (Supplemental Figure 6). All three members of the *PpTAS3a/d/f* clade have upstream flanking regions that produce miR156 and/or miR529-sliced RNAs, in at least two cases (*PpTAS3a*/*PpTAS6a* and *PpTAS3f*/*PpTAS6b*) corresponding with the production of phased *DCL4*/*RDR6*-dependent siRNAs. Despite the fact that *PpTAS6a* and *PpTAS6b* do not share sequence similarity in their siRNA-generating regions, their common arrangement proximal to *PpTAS3* loci and their shared presence of sliced miR156 sites strongly suggest a common ancestry that we believe justifies their classification into the same family. We have yet to observe siRNA accumulation from *PpTAS6c*, so this annotation should be regarded as provisional.

We used all 248 *PpTAS6a* and *PpTAS6b*-derived siRNAs from our wild-type sequencing data as queries for ta-siRNA target predictions using a standard scoring matrix (Allen et al., 2005). One hundred and fifty target sites, from 129 distinct transcripts, were predicted with alignment scores of 3.5 or less (Supplemental Table 4). At the present time, we have low confidence in these predictions, as the cohort of transcripts did not seem to have a coherent functional theme, and none of these predictions was supported by robust evidence of slicing in the available degradome data. We did identify robust degradome data supporting the slicing of a zinc-finger domain transcript by a *PpTAS6a*-derived siRNA with a higher alignment score (5.5; Figure 5B). While this alignment score is relatively high, we note that the siRNA target mismatches are concentrated on the 3′ end of the complementary region and that the degradome data strongly support the *in vivo* accumulation of the predicted slicing remnant. We conclude that at least one *PpTAS6a* ta-siRNA, which we name ta-siZNF, is functional in slicing a zinc-finger domain transcript *in trans*, and that other *trans* targets may exist for other *PpTAS6*-derived siRNAs.

DISCUSSION

The most striking features of the Δ*PpDCL4* mutants are the pleiotropic defects throughout vegetative development and sterility. The defects in the vegetative development include developmental programs such as gametophore elongation,

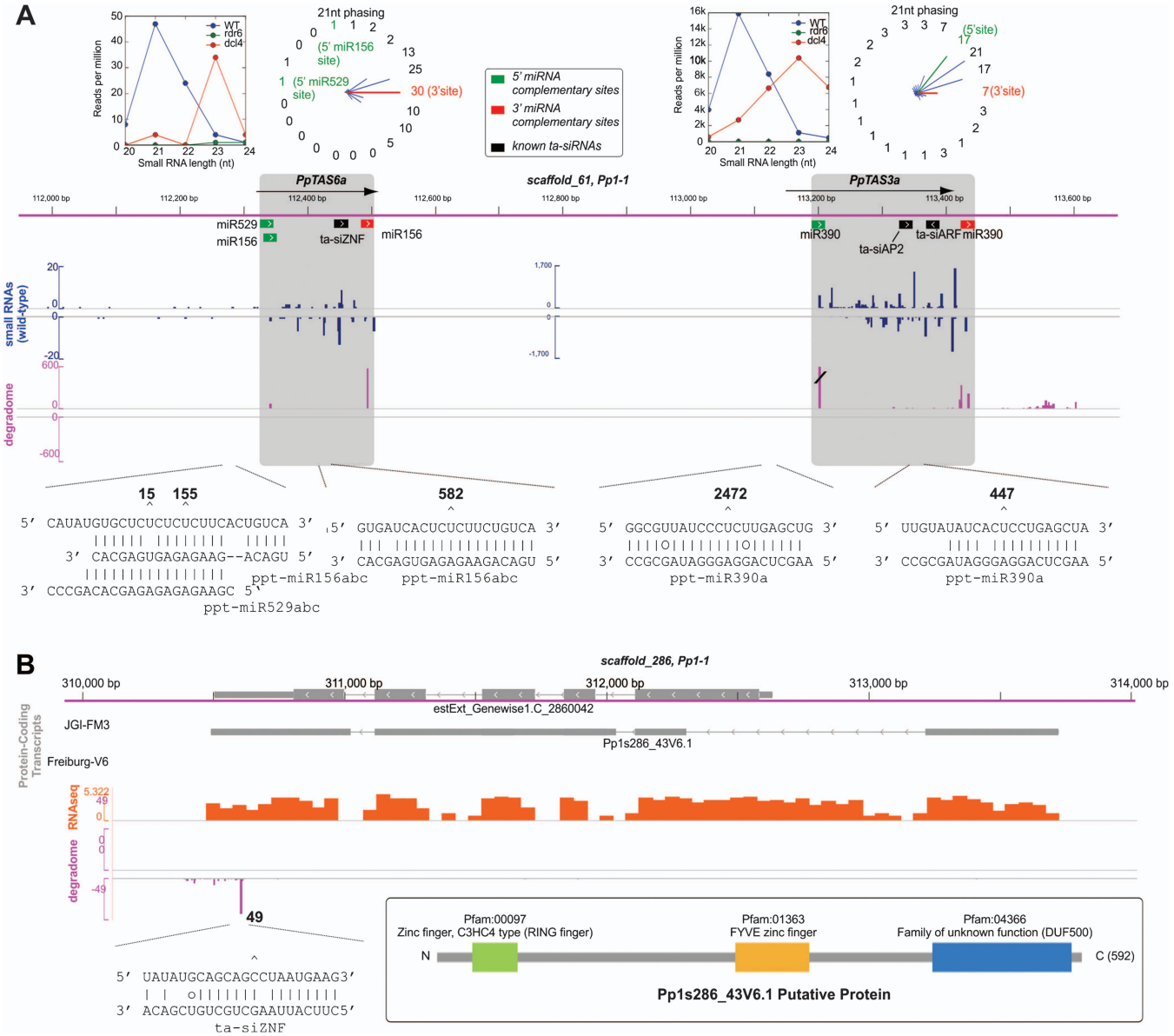

Figure 5. Neighboring miR156- and miR390-Sliced TAS Loci.
(A) An annotated genomic snapshot of *PpTAS3a* and *PpTAS6a*. Shaded regions indicate boundaries of indicated *TAS* loci, with locations and strand orientations of miRNA complementary sites and known functional ta-siRNAs shown. Insets above show the small RNA size distribution in the indicated genotypes, as well as the 'phasing' distributions of wild-type small RNAs in 21-nt bins (numbers on periphery indicate percentage of siRNAs in each bin). Browser track small RNA data (blue) and degradome data (magenta) show the 5′ end positions from wild-type samples, with positive values indicating Watson-strand mapped reads, and negative values indicating Crick-strand mapped reads. Insets below show miRNAs aligned with miRNA complementary sites. Numbers above alignments are the number of degradome-derived 5′ ends mapped to the 10th nucleotide of the alignment.
(B) Evidence for *trans*-acting slicing directed by the *PpTAS6a*-derived ta-siZNF. Annotated genomic snapshot showing protein-coding transcripts (gray), polyA+ RNAseq data (not strand-specific (Zemach et al., 2010), and degradome data. Inset below-left shows ta-siZNF/target alignment, with the number of degradome reads at the 10th nucleotide of the alignment indicated. Inset below-right shows schematic of the protein (from Phytozome).

protonema and leaf development, as well as specific growth programs linked to altered physiological conditions. Δ*PpDCL4* mutants fail to develop caulonema filaments with a negative gravitropic growth in darkness and they form numerous brachycytes that usually only develop in response to abiotic stress conditions in *Physcomitrella* wild-type. The enhanced brachycyte development could either be due to the constitutive activation of the underlying developmental program or could result from an altered plant physiology causing abiotic stress symptoms that result in the onset of stress-associated

Table 1. Summary of *Physcomitrella DCL4/RDR6*-Dependent *TAS* Loci.

Locus	5′ miR390 site	3′ miR390 site	5′ miR529 site	5′ miR156 site	3′ miR156 site	ta-siAP2	ta-siARF	ta-siZNF
PpTAS3a/PpTAS6a	S	S	S	S	S	+	+	+
PpTAS3b	P	P	N/A	N/A	N/A	+	+	N/A
PpTAS3c	S	S	N/A	N/A	N/A	–	+	N/A
PpTAS3d/PpTAS6c	S	S	P	S	S	+	+	Absent
PpTAS3e	S	S	N/A	N/A	N/A	–	+	N/A
PpTAS3f/PpTAS6b	S	S	P	P	S	+	+	Absent

S, degradome-based evidence of slicing; P, predicted miRNA target site w/o degradome evidence; +, ta-siRNA pairs well with one or more target; –, ta-siRNA does not pair well (score ⩾ 6) with any targets; N/A, not applicable; absent, site or ta-siRNA not found within locus.

pathways and brachycyte formation. Even though we did not detect morphological differences of antheridia and archegonia in Δ*PpDCL4* mutants, the cross-fertilization experiment with wild-type plants indicated at least female sterility.

At the molecular level, we found that *PpDCL4* is essential for the accumulation of 21-nt ta-siRNAs from *TAS* transcripts corresponding to the function of DCL4 orthologs in *Arabidopsis* and rice (Gasciolli et al., 2005; Liu et al., 2007). Loss of PpDCL4 function allowed PpDCL4 substrates to be processed instead by PpDCL3, leading to the accumulation of off-sized, 23–24-nt siRNAs in the Δ*PpDCL4* mutant. Such conditional *DCL* redundancy upon *TAS* substrates has also been observed in rice and *Arabidopsis dcl4* mutants (Gasciolli et al., 2005; Liu et al., 2007). In all cases, a *DCL3* homolog becomes competent for ta-siRNA biogenesis upon the loss of *DCL4* function. Concerning this, *Physcomitrella* differs from rice and *Arabidopsis* only in that *Physcomitrella* lacks the *DCL2* homolog that in rice and *Arabidopsis* also contributes to ta-siRNA production upon loss of *DCL4* function. Our evidence suggests that the *PpDCL3*-dependent ta-siRNAs that arise in the Δ*PpDCL4* plants are functional *in cis*: *TAS* primary transcripts are reduced concomitant with an increase in DNA methylation at *TAS* chromatin.

The dramatic morphological defects seen in Δ*PpDCL4* plants cannot be attributed solely to reduced ta-siRNA accumulation. Δ*PpRDR6* plants completely lack all known ta-siRNAs (Talmor-Neiman et al., 2006; Cho et al., 2008) but nonetheless have a very mild phenotype consisting of an accelerated rate of transition from the filamentous protonematal growth stage to the leafy gametophore stage. The morphological phenotypes apparent in Δ*PpDCL4* plants require the activity of *PpDCL3*, as the Δ*PpDCL3*/Δ*PpDCL4* double-mutant plants resemble the comparatively mild growth changes seen in Δ*PpRDR6*. Thus, the role that *PpDCL3* plays in the Δ*PpDCL4* background appears to be specifically detrimental to normal *Physcomitrella* development. A similar observation has been made in *Arabidopsis* where ta-siRNAs of aberrant sizes are made by DCL2 and DCL3 in the absence of DCL4, and *dcl1/dcl4* double mutants exhibit pleiotropic developmental defects absent in the *dcl1/dcl2/dcl4* triple mutant (Bouche et al., 2006). These data imply that, as in the case of *Physcomitrella* DCL3, ectopic DCL2 activity in *Arabidopsis* can trigger dramatic phenotypic consequences. However, compensatory or ectopic DCL activities do not always cause major phenotypes. The phase-change and polarity defects of *Arabidopsis dcl4* mutants are enhanced, not eliminated, in *dcl3/dcl4* mutants and these defects are identical to those observed in *rdr6* mutants (Gasciolli et al., 2005). *Oryza dcl3dcl4* double mutants have not been reported. However, the strong phenotypes observed in *OsDCL4* (*SHO1*) mutants are identical to those seen in plants defective in the rice *RDR6* homolog, *SHL2* (Nagasaki et al., 2007), strongly suggesting that reduction of ta-siRNA accumulation, not the effects of compensatory *DCLs*, underlies the phenotypes observed in *OsDCL4* mutant plants.

Why might *PpDCL3* activity have such dramatic effects in the *PpDCL4* background? The distinct phenotype seems likely to be explained by the regulatory activities of the *PpDCL3*-dependent off-sized ta-siRNAs that arise solely in this background. These off-sized ta-siRNAs may target RNAs that are not under sRNA control in wild-type, and/or regulate normal ta-siRNA targets with an unusual strength or via different molecular mechanisms. Representatives of two known 'normal' ta-siRNA targets were up-regulated in the Δ*PpDCL4* background, suggesting that perhaps other targets of the 'off-sized' ta-siRNAs cause the Δ*PpDCL4* phenotype. To address this question, we performed target predictions for all 23–24-nt ta-siRNAs arising from the *PpTAS3a* precursor (Supplemental Table 2). Among the predicted targets, we find transcripts encoding proteins that were previously shown to control developmental processes and the misregulation of which could account for the developmental defects in the Δ*PpDCL4* mutant. For example, auxin triggers specific developmental steps in *P. patens* (Ludwig-Muller et al., 2009) and we identified putative off-sized ta-siRNA target transcripts encoding proteins that are involved in auxin transport and signaling as well as auxin-induced downstream transcripts. One putative off-sized ta-siRNA target (*Pp1s42_203V6.1*) encodes a homolog of *A. thaliana* BIG, a calossin-like protein required for polar auxin transport (Gil et al., 2001). Two other predicted targets (*Pp1s74_86V6.1* and *Pp1s5_432V6.1*) are homologs of auxin-regulated *AP2/EREBP* genes, which control cell division patterning at early stages of root primordium development in *A. thaliana* (Hirota et al., 2007). Another putative off-sized ta-siRNA target (*Pp1s220_89V6.1*) encodes a homolog of the

A. thaliana N-MYC down-regulated-like 2 (NDL2) protein that acts in the auxin signaling pathway and down-regulation of members of the NDL family was shown to alter root architecture in *A. thaliana* (Mudgil et al., 2009). Additional targets were predicted that do not act in auxin-responsive pathways but have an impact on the development of plants. For example, one of the predicted targets (*Pp1s60_37V6.1*) encodes a protein homologous to MOS1 (modifier of snc1) from *A. thaliana* that controls the expression of SUPPRESSOR OF npr1-1 CONSTITUTIVE1 (SNC1). *mos1* mutants show retarded growth and it was suggested that MOS1 regulates gene expression at the chromatin level (Li et al., 2010). Another predicted target (*Pp1s642_3V6.1*) encodes a A-type cyclin (CYCA1) homolog that is involved in meiotic division in *A. thaliana*. *cyca1* mutants fail to enter meiosis II and consequently produce diploid spores (d'Erfurth et al., 2010). In addition, two homologs (*Pp1s42_258V6.1* and *Pp1s336_16V6.1*) of *HAP6* from *A. thaliana* were predicted as off-sized ta-siRNA targets that act in pollen grain development, since pollen grains of *A. thaliana hap6* mutants cannot fertilize properly (Johnson et al., 2004). The sterility defects observed in Δ*PpDCL4* mutants may be attributed to the down-regulation of the *PpCYCA1* and/or *PpHAP6* homologs.

An alternative possibility is that off-sized, *DCL3*-dependent miRNAs from *MIRNA*s normally processed by PpDCL4 are responsible for the phenotypes of Δ*PpDCL4* plants. Although we cannot rule out this possibility completely, our RNA blot and smallRNAseq analyses found no evidence for *PpDCL4*-dependent miRNAs nor evidence for off-sized miRNA accumulation in the Δ*PpDCL4* background. Future experiments should seek to understand the molecular basis for the *PpDCL3*-dependent phenotypes observed in the Δ*PpDCL4* background.

In *Arabidopsis* (Howell et al., 2007) and *Physcomitrella* genome, only a limited number of endogenous *DCL4*/*RDR6*-dependent small RNA loci have been identified. Our analysis of *DCL4*/*RDR6*-dependent loci in *Physcomitrella* has revealed several interesting findings. All of the *Physcomitrella DCL4*/*RDR6*-dependent siRNAs appear to derive from primary transcripts sliced at least once, and often several times, by a miRNA(s). We describe a new family of *TAS* loci that are associated with miR156- and miR529-directed slicing. miR156 is an ancient plant miRNA that has a cohort of conserved, protein-coding targets independently of *TAS* loci. In all plant species examined, including *Physcomitrella*, miR156 targets mRNAs encoding *Squamosa Promoter Binding Like* (*SBP*/*SPL*) transcription factors (Poethig, 2009). In angiosperms, miR156-mediated regulation of *SBP*/*SPL* targets is critical for many distinct aspects of developmental timing (Wu and Poethig, 2006; Wu et al., 2009; Nodine and Bartel, 2010). However, miR156-associated *TAS* loci have not been previously described in any plant species. miR529 is related in sequence to miR156, and also widely conserved. At least one *PpTAS6*-derived siRNA appears to be a true ta-siRNA, in that we could identify a sliced zinc-finger domain target. The *PpTAS6* family is also unique in its very close proximity to miR390-targeted *PpTAS3* loci; the three *TAS3*/*TAS6* pairs are separated by only ~0.7 kb, and their miRNA complementary sites are all on the same strands. This suggests that these *PpTAS6*/*PpTAS3* pairs could share single common primary transcripts, and that miR156-, miR529-, and miR390-mediated activities may be interrelated in *Physcomitrella*.

Our findings demonstrate ta-siRNA biogenesis mechanisms in *Physcomitrella* and the existence of additional *TAS* precursors. This indicates that ta-siRNA-regulated mechanisms are much more complex than thought before, and opens new avenues for investigating the molecular mechanisms that control small RNA-directed developmental processes.

METHODS

Plant Material and Phenotypic Analysis

Physcomitrella cultivation, sporophyte induction, protoplast isolation, PEG-mediated transformation, and regeneration of stably transformed plants were performed according to standard procedures (Frank et al., 2005). The lines reported in this study are deposited in the International Moss Stock Center (IMSC, www.moss-stock-center.org) with the accession numbers IMSC 40436–40437 (Δ*PpDCL4* mutants), IMSC 40433 (Δ*PpDCL3* mutant), and IMSC 40440, 40441, 40552, 40553, 40555, 40556 (Δ*PpDCL3*/Δ*PpDCL4* double mutants). Pictures of plants were taken with either a KAISER Scan Do scanner (Buchen, Germany) or a Zeiss Axioplan 2 microscope fitted with an Axiocam MRc5 (Zeiss, Jena). For caulonema induction, 5-μl droplets from freshly dispersed liquid cultures with an adjusted density of 100 mg L^{-1} dry weight were spotted onto solid growth medium. The plates were sealed and cultivated under standard growth conditions for 3 weeks. Subsequently, the plates were wrapped in aluminum foil, positioned vertically, and cultured for another 8 days.

Isolation of *PpDCL3* and *PpDCL4* Full-Length cDNA

PpDCL3 and *PpDCL4* were initially identified by TBLASTN searches in *Physcomitrella* EST sequences (Rensing et al., 2002) using *Arabidopsis* DCL1-4 protein sequences (accession numbers P84634, Q9SP32, NP_189978, NP_566199) as queries. The isolation of full-length cDNA sequences was performed by 5'RACE-PCR, 3'RACE-PCR, and RT-PCR using primers deduced from *Physcomitrella* genomic sequence data. To confirm that PCR products were derived from the same cDNA, all PCR and RACE primers were selected to produce overlapping PCR fragments. The sequences were assembled and full-length *PpDCL3* and *PpDCL4* cDNA sequences were submitted to GenBank with accession numbers EF670437 and EF670438, respectively. The Pfam database (Finn et al., 2008) was used for protein domain predictions.

Generation of Δ*PpDCL4* Mutant Lines

A zeocin selection marker cassette was cloned into a single restriction site present in a *PpDCL4* genomic fragment. The gene disruption construct was transfected into *Physcomitrella*

protoplasts and zeocin-resistant lines were analyzed by PCR and genomic DNA blot to confirm precise integration into the *PpDCL4* locus. Loss of *PpDCL4* transcript was confirmed by RT–PCR. The generation of *ΔPpDCL4* mutants is described in detail in Supplemental Material and Methods.

Generation of Δ*PpDCL3*/Δ*PpDCL4* Double Mutants

An *nptII* (neomycin phosphotransferase II) expression cassette (Strepp et al., 1998) was cloned into the PAZ domain encoding region of *PpDCL3*, transfected into wild-type protoplasts, and G418-resistant lines were analyzed by PCR and genomic DNA blot to confirm precise integration into the *PpDCL3* locus. Loss of *PpDCL3* transcript was confirmed by RT–PCR. Δ*PpDCL3* mutant protoplasts were subsequently transfected with the *PpDCL4* knockout construct where the zeocin selection cassette was replaced by *hpt* (hygromycin phosphotransferase) resistance cassette (Huether et al., 2005). Antibiotic resistant lines were analyzed by PCR for proper insertion of the *PpDCL4* knockout construct. RT–PCR analyses of these lines confirmed the loss of *PpDCL3* and *PpDCL4* transcripts (Δ*PpDCL3*/Δ*PpDCL4*). The generation of Δ*PpDCL3*/Δ*PpDCL4* double mutants is described in detail in Supplemental Material and Methods.

Small RNA Sequencing and Data Analysis

Total RNA was isolated from 10-day-old protonema from Δ*PpDCL4* mutants and wild-type plants as previously described (Cho et al., 2008). Small RNAs (~10–40 nt) were recovered by PAGE fractionation. Small RNA sequencing libraries for the Applied Biosystems SOLiD™ 2 system were prepared using the SOLiD™ small RNA expression kit (Ambion) according to the manufacturer's instructions. Barcoded libraries were sequenced using a SOLiD™ 2 system. Barcoded color space data were first parsed to separate different samples mixed in the same run. Barcode-sorted color space reads (35 colors) were then parsed to identify the first five nucleotides of the constant 3′ adapter. The adapter sequences were trimmed. Only reads with sizes of 20–24 nt were retained and were directly translated to DNA space. The processed and raw data are available from the Gene Expression Omnibus (GEO: Accession GSE18466). The processed reads were mapped to the *Physcomitrella* genome as previously described (Cho et al., 2008), retaining only exact matches. Custom PERL scripts were used to analyze small RNA expression from *MIRNA* and *TAS* loci.

Identification of Additional *TAS* Loci

SmallRNAseq data from *Physcomitrella* wild-type (GSM115095, GSM115096, GSM115097, GSM313212, and GSM313213), *dcl3* (GSM313214, GSM313215), and *rdr6* (GSM313216, GSM313217) was previously described (Axtell et al., 2006; Cho et al., 2008) and the smallRNAseq library from *dcl4* mutant current study (GSM459911) was used in the analysis. 20–24-nt small RNAs from each of the 10 libraries were mapped to the *Physcomitrella* genome (v1.1) using bowtie (Langmead et al., 2009), v0.12.7, with settings '-v 1 -a –best –strata -f -p 7 -k 100' as well as '-C' for color space data. Therefore, mappings with either zero or one mismatch were accepted and, for reads that had more than 100 optimal mapping positions, only the first 100 were reported. Reads mapping to rRNA, tRNA, or *MIRNA* hairpin positions were then discarded. The total small RNA abundance in 200-nt non-overlapping bins was calculated genome-wide, and scaled to reads per million to facilitate comparisons between different datasets. The top 1000 most abundant bins in the wild-type datasets were then screened to find bins meeting the following criteria: (1) symmetry (defined as the proportion of small RNAs mapped to one or the other strand) of 0.25–0.75, (2) *rdr6* total $<0.2\times$ wild-type total, (3) percentage 21–22-nt RNAs in wild-type and *dcl3* $>70\%$, and (4) percentage 23–24-nt RNAs in *dcl4* $>50\%$. These parameters were inferred from the characteristics of the previously known *PpTAS3a–d* loci. The three novel bins that passed this filter were then further examined by searching for miRNA complementary sites (based on BLASTN) within a centered 1000-nt window. The final annotations of these three novel loci, *PpTAS3e*, *PpTAS3f*, and *PpTAS6a*, were based on manual curation and the positions of the miRNA complementary sites. *PpTAS6b* did not pass the initial computational filter but was identified serendipitously based upon its proximity to *PpTAS3f*. Similarly, *PpTAS6c* lacked corresponding siRNAs in our dataset but was identified based on proximity to *PpTAS3d* and the presence of miR156 target sites. The siRNA population may be generated from *PpTAS6c* under different physiological conditions or different tissue types. Degradome sequencing data from *Physcomitrella* have been previously described (Addo-Quaye et al., 2009). CleaveLand 2 (Ma et al., 2010) was used for degradome analysis. For siRNA target predictions, we used axtell_targetfinder.pl (Ma et al., 2010). Phylogenetic analysis of *PpTAS3a-f* utilized a MUSCLE alignment (Edgar, 2004) of the regions between the miR390 complementary sites as input to the Maximum Likelihood method in MEGA5 based on the Tamura-Nei model (Tamura and Nei, 1993). The bootstrap consensus tree, based on 500 replicates, was shown. A .bed file has been created (Supplemental Table 5) that indicates genomic locations of *Physcomitrella TAS* loci (genome assembly version 1.1) as well as important features within the *TAS* loci.

Detection of Small RNAs by RNA Gel Blots

Total RNA was separated in a 13% polyacrylamide gel containing 8.3 M urea in 1 TBE buffer and electro-blotted onto nylon membranes for 1 h at 400 mA. Oligonucleotides complementary to miRNA, ta-siRNA and U6snRNA sequences were radiolabeled with [γ-^{32}P]ATP using T4 polynucleotide kinase (Fermentas). Blot hybridization was carried out in buffer containing 0.05 M sodium phosphate (pH 7.2), 1 mM EDTA, 6 SSC, 1 Denhardt's and 5% SDS. Blots were washed two to three times with 2 SSC, 0.2% SDS, and one time with 1 SSC, 0.1% SDS. Blots were hybridized and washed at temperatures 10°C below the T_m of the oligonucleotide. Sequences of oligonucleotides used for the detection of small RNAs are listed in Supplemental Table 6.

Detection of RNA Cleavage Products

RNA ligase mediated 5′ RACE PCR was performed with a modified GeneRacer Kit (Invitrogen) protocol (Llave et al., 2002). PCR reactions were performed using the GeneRacer forward primer 5′-CGACTGGAGCACGAGGACACTGA-3′ and the *PpARF* (*Phypa_203442*) gene-specific primer 5′-CACTCGACACGTCGTTGCTGAGAGTT-3′ followed by a PCR with the nested GeneRacer forward primer 5′-GGACACTGACATGGACTGAAGGAGTA-3′ and the nested gene-specific primer 5′-ATGAGGAGGTCCGGGAGGATTCGATA-3′. Amplification products corresponding to the size of expected cleavage products were excised from the gel, cloned, and sequenced.

Expression Analysis by Quantitative Real-Time PCR

RNA was extracted from three biological replicates of *Physcomitrella* wild-type and two Δ*PpDCL4* mutant lines with TRIzol reagent (Invitrogen), treated with DNase I (Fermentas), and reverse-transcribed into first-strand cDNA by Taq Man Reverse Transcription Reagents (Applied Biosystems). Real-time PCR was performed on a Roche 480 Light Cycler using gene-specific primers and Light Cycler 480 SYBR Green I Master (Roche) according to the manufacturer's instructions. The constitutively expressed gene *PpEF1α* was used as reference gene for normalization. Expression levels of *PpAP2* (*Phypa_65352*) and *PpARF* (*Phypa_203442*) were calculated relative to transcript abundance in wild-type employing relative quantification with efficiency correction (Livak and Schmittgen, 2001). Primer sequences are reported in Supplemental Table 6.

DNA Methylation Analysis

Two μg of genomic DNA from wild-type and two Δ*PpDCL4* mutant lines were treated with sodium bisulfite using the EpiTect Bisulfite Kit (Qiagen). *TAS3a* and *TAS3c* sequences were analyzed with the MethPrimer program (Li and Dahiya, 2002) to deduce methylation-specific (MSP) and unmethylation-specific primers (USP) for PCR analysis of bisulfite-treated DNA. PCR products were cloned using the CloneJET PCR Cloning Kit (Fermentas) and sequenced. Primer sequences are reported in Supplemental Table 6.

Target Prediction

The targets of 23–24-nt ta-siRNAs generated from *PpTAS3a* precursor were predicted against the *Physcomitrella* mRNAs (from Phytozome 7.0; dataset 'Ppatens_152_transcript.fa') using the Carrington Lab script 'targetfinder.pl' (http://carringtonlab.org/resources/targetfinder). It is based on Allen's parameters and only targets that gave a maximum score of 4.0 were considered as true targets (Allen et al., 2005; Fahlgren et al., 2007).

Phylogenetic Analysis

The sense-strand sequences between the two miR390 complementary sites for each of the six *PpTAS3* loci were aligned using MUSCLE 3.8 (Edgar, 2004) using default parameters. The resulting FASTA-formatted alignment used for phylogenetic analysis is listed in Supplemental Table 7. Phylogenetic analysis was performed using MEGA 5.05 for Mac OSX (Tamura et al., 2011). The bootstrap consensus tree from a maximum likelihood reconstruction (Nucleotide substitution model (Tamura and Nei, 1993); Uniform rates among sites; gaps treated as complete deletion; NNI ML heuristic method with automatic initial tree) using 1000 bootstrap replicates is shown in Supplemental Figure 6. Nodes with less than 100% bootstrap support are annotated with percent support. Scale bar: substitutions per site (n = 103 informative sites).

SUPPLEMENTARY DATA

Supplementary Data are available at *Molecular Plant Online.*

FUNDING

This work was supported by Landesstiftung Baden-Württemberg (P-LS-RNS/40 to W.F. and R.R.), the German Federal Ministry of Education and Research (FRISYS 0313921 to R.R. and W.F.), the German Academic Exchange Service (DAAD; Ph.D. fellowship to M.A.A. and I.F.), the graduate school GRK1305 (Ph.D. fellowship to A.K.B.), and the US National Institutes of Health (R01GMR084051 to M.J.A.).

ACKNOWLEDGMENTS

We thank Jo Ann Snyder for assistance with moss propagation; Jim Carrington and Blake Meyers for discussion on *TAS* nomenclature; and Jeff Duckett and Jan-Peter Frahm for discussions on the morphology of mutant lines. Author contributions: M.A.A. generated and analyzed Δ*PpDCL4* and Δ*PpDCL3*/Δ*PpDCL4* mutants; I.F. and A.K.B. helped in the analysis of Δ*PpDCL4* mutants; M.J.A. and S.H.C. performed sRNA sequencing; M.J.A. and Z.M. analyzed sRNA sequencing data and annotated novel *TAS* loci; W.F. designed research; M.A.A., M.J.A., and W.F. analyzed the data; and M.A.A. and W.F. wrote the paper with support from R.R., A.K.B., S.H.C., and M.J.A. No conflict of interest declared.

REFERENCES

Addo-Quaye, C., Snyder, J.A., Park, Y.B., Li, Y.F., Sunkar, R., and Axtell, M.J. (2009). Sliced microRNA targets and precise loop-first processing of MIR319 hairpins revealed by analysis of the *Physcomitrella patens* degradome. RNA. **15,** 2112–2121.

Adenot, X., et al. (2006). DRB4-dependent TAS3 *trans*-acting siRNAs control leaf morphology through AGO7. Curr. Biol. **16,** 927–932.

Allen, E., Xie, Z., Gustafson, A.M., and Carrington, J.C. (2005). microRNA-directed phasing during *trans*-acting siRNA biogenesis in plants. Cell. **121,** 207–221.

Axtell, M.J., Jan, C., Rajagopalan, R., and Bartel, D.P. (2006). A two-hit trigger for siRNA biogenesis in plants. Cell. **127,** 565–577.

Axtell, M.J., Snyder, J.A., and Bartel, D.P. (2007). Common functions for diverse small RNAs of land plants. Plant Cell. **19,** 1750–1769.

Borsani, O., Zhu, J., Verslues, P.E., Sunkar, R., and Zhu, J.K. (2005). Endogenous siRNAs derived from a pair of natural *cis*-antisense

transcripts regulate salt tolerance in *Arabidopsis*. Cell. **123,** 1279–1291.

Bouche, N., Lauressergues, D., Gasciolli, V., and Vaucheret, H. (2006). An antagonistic function for *Arabidopsis* DCL2 in development and a new function for DCL4 in generating viral siRNAs. EMBO J. **25,** 3347–3356.

Chan, S.W., Henderson, I.R., and Jacobsen, S.E. (2005). Gardening the genome: DNA methylation in *Arabidopsis thaliana*. Nat. Rev. Genet. **6,** 351–360.

Cho, S.H., et al. (2008). *Physcomitrella patens* DCL3 is required for 22–24 nt siRNA accumulation, suppression of retrotransposon-derived transcripts, and normal development. PLoS Genet. **4,** e1000314.

d'Erfurth, I., et al. (2010). The cyclin-A CYCA1;2/TAM is required for the meiosis I to meiosis II transition and cooperates with OSD1 for the prophase to first meiotic division transition. PLoS Genet. **6,** e1000989.

Decker, E.L., Frank, W., Sarnighausen, E., and Reski, R. (2006). Moss systems biology en route: phytohormones in *Physcomitrella* development. Plant Biol. Stuttg. **8,** 397–405.

Deleris, A., Gallego-Bartolome, J., Bao, J., Kasschau, K.D., Carrington, J.C., and Voinnet, O. (2006). Hierarchical action and inhibition of plant Dicer-like proteins in antiviral defense. Science. **313,** 68–71.

Du, T., and Zamore, P.D. (2005). microPrimer: the biogenesis and function of microRNA. Development. **132,** 4645–4652.

Dunoyer, P., Himber, C., and Voinnet, O. (2005). DICER-LIKE 4 is required for RNA interference and produces the 21-nucleotide small interfering RNA component of the plant cell-to-cell silencing signal. Nat. Genet. **37,** 1356–1360.

Edgar, R.C. (2004). MUSCLE: multiple sequence alignment with high accuracy and high throughput. Nucleic Acids Res. **32,** 1792–1797.

Fahlgren, N., et al. (2007). High-throughput sequencing of *Arabidopsis* microRNAs: evidence for frequent birth and death of *MIRNA* genes. Plos ONE. **2,** e219.

Fahlgren, N., et al. (2009). Computational and analytical framework for small RNA profiling by high-throughput sequencing. RNA. **15,** 992–1002.

Finn, R.D., et al. (2008). The Pfam protein families database. Nucleic Acids Res. **36,** D281–D288.

Frank, W., Decker, E.L., and Reski, R. (2005). Molecular tools to study *Physcomitrella patens*. Plant Biol. Stuttg. **7,** 220–227.

Gasciolli, V., Mallory, A.C., Bartel, D.P., and Vaucheret, H. (2005). Partially redundant functions of *Arabidopsis* DICER-like enzymes and a role for DCL4 in producing *trans*-acting siRNAs. Curr. Biol. **15,** 1494–1500.

Gil, P., et al. (2001). BIG: a calossin-like protein required for polar auxin transport in *Arabidopsis*. Genes Dev. **15,** 1985–1997.

Goll, M.G., and Bestor, T.H. (2005). Eukaryotic cytosine methyltransferases. Annu. Rev. Biochem. **74,** 481–514.

Henderson, I.R., et al. (2006). Dissecting *Arabidopsis thaliana* DICER function in small RNA processing, gene silencing and DNA methylation patterning. Nat. Genet. **38,** 721–725.

Herr, A.J., Jensen, M.B., Dalmay, T., and Baulcombe, D.C. (2005). RNA polymerase IV directs silencing of endogenous DNA. Science. **308,** 118–120.

Hirota, A., Kato, T., Fukaki, H., Aida, M., and Tasaka, M. (2007). The auxin-regulated AP2/EREBP gene PUCHI is required for morphogenesis in the early lateral root primordium of *Arabidopsis*. Plant Cell. **19,** 2156–2168.

Hohe, A., Rensing, S.A., Mildner, M., Lang, D., and Reski, R. (2002). Day length and temperature strongly influence sexual reproduction and expression of a novel MADS-box gene in the moss *Physcomitrella patens*. Plant Biol. **4,** 595–602.

Howell, M.D., et al. (2007). Genome-wide analysis of the RNA-DEPENDENT RNA POLYMERASE6/DICER-LIKE4 pathway in *Arabidopsis* reveals dependency on miRNA- and tasiRNA-directed targeting. Plant Cell. **19,** 926–942.

Huether, C.M., et al. (2005). Glyco-engineering of moss lacking plant-specific sugar residues. Plant Biol. **7,** 292–299.

Johnson, M.A., et al. (2004). *Arabidopsis* hapless mutations define essential gametophytic functions. Genetics. **168,** 971–982.

Kasschau, K.D., et al. (2007). Genome-wide profiling and analysis of *Arabidopsis* siRNAs. PLoS Biol. **5,** e57.

Khraiwesh, B., et al. (2010). Transcriptional control of gene expression by microRNAs. Cell. **140,** 111–122.

Langmead, B., Trapnell, C., Pop, M., and Salzberg, S.L. (2009). Ultrafast and memory-efficient alignment of short DNA sequences to the human genome. Genome Biol. **10,** R25.

Li, F., Orban, R., and Baker, B. (2012). SoMART, a web server for plant miRNA, tasiRNA and target gene analysis. Plant J. doi: 10.1111/j.1365–313X.2012.04922.x.

Li, L.C., and Dahiya, R. (2002). MethPrimer: designing primers for methylation PCRs. Bioinformatics. **18,** 1427–1431.

Li, Y., Tessaro, M.J., Li, X., and Zhang, Y. (2010). Regulation of the expression of plant resistance gene SNC1 by a protein with a conserved BAT2 domain. Plant Physiol. **153,** 1425–1434.

Lister, R., et al. (2008). Highly integrated single-base resolution maps of the epigenome in *Arabidopsis*. Cell. **133,** 523–536.

Liu, B., et al. (2007). *Oryza sativa* dicer-like4 reveals a key role for small interfering RNA silencing in plant development. Plant Cell. **19,** 2705–2718.

Livak, K.J., and Schmittgen, T.D. (2001). Analysis of relative gene expression data using real-time quantitative PCR and the $2^{-\Delta\Delta C_T}$ Method. Methods. **25,** 402–408.

Llave, C., Xie, Z., Kasschau, K.D., and Carrington, J.C. (2002). Cleavage of Scarecrow-like mRNA targets directed by a class of *Arabidopsis* miRNA. Science. **297,** 2053–2056.

Lu, C., et al. (2006). MicroRNAs and other small RNAs enriched in the *Arabidopsis* RNA-dependent RNA polymerase-2 mutant. Genome Res. **16,** 1276–1288.

Ludwig-Muller, J., Decker, E.L., and Reski, R. (2009). Dead end for auxin conjugates in Physcomitrella? Plant Signal Behav. **4,** 116–118.

Ma, Z., Coruh, C., and Axtell, M.J. (2010). *Arabidopsis* lyrata small RNAs: transient MIRNA and small interfering RNA loci within the *Arabidopsis* genus. Plant Cell. **22,** 1090–1103.

Margis, R., et al. (2006). The evolution and diversification of Dicers in plants. FEBS Lett. **580,** 2442–2450.

Montgomery, T.A., et al. (2008). Specificity of ARGONAUTE7-miR390 interaction and dual functionality in TAS3 *trans*-acting siRNA formation. Cell. **133,** 128–141.

Mudgil, Y., Uhrig, J.F., Zhou, J., Temple, B., Jiang, K., and Jones, A.M. (2009). *Arabidopsis* N-MYC DOWNREGULATED-LIKE1, a positive regulator of auxin transport in a G protein-mediated pathway. Plant Cell. **21,** 3591–3609.

Nagasaki, H., et al. (2007). The small interfering RNA production pathway is required for shoot meristem initiation in rice. Proc. Natl Acad. Sci. U S A. **104,** 14867–14871.

Nodine, M.D., and Bartel, D.P. (2010). MicroRNAs prevent precocious gene expression and enable pattern formation during plant embryogenesis. Genes Dev. **24,** 2678–2692.

Park, W., Li, J., Song, R., Messing, J., and Chen, X. (2002). CARPEL FACTORY, a Dicer homolog, and HEN1, a novel protein, act in microRNA metabolism in *Arabidopsis thaliana*. Curr. Biol. **12,** 1484–1495.

Peragine, A., Yoshikawa, M., Wu, G., Albrecht, H.L., and Poethig, R.S. (2004). SGS3 and SGS2/SDE1/RDR6 are required for juvenile development and the production of *trans*-acting siRNAs in *Arabidopsis*. Genes Dev. **18,** 2368–2379.

Poethig, R.S. (2009). Small RNAs and developmental timing in plants. Curr. Opin. Genet. Dev. **19,** 374–378.

Qi, Y., and Hannon, G.J. (2005). Uncovering RNAi mechanisms in plants: biochemistry enters the foray. FEBS Lett. **579,** 5899–5903.

Rajagopalan, R., Vaucheret, H., Trejo, J., and Bartel, D.P. (2006). A diverse and evolutionarily fluid set of microRNAs in *Arabidopsis thaliana*. Genes Dev. **20,** 3407–3425.

Reinhart, B.J., Weinstein, E.G., Rhoades, M.W., Bartel, B., and Bartel, D.P. (2002). MicroRNAs in plants. Genes Dev. **16,** 1616–1626.

Rensing, S.A., Rombauts, S., Van de Peer, Y., and Reski, R. (2002). Moss transcriptome and beyond. Trends Plant Sci. **7,** 535–538.

Reski, R. (1998). Development, genetics and molecular biology of mosses. Bot. Acta. **111,** 1–15.

Ruby, J.G., et al. (2006). Large-scale sequencing reveals 21U-RNAs and additional microRNAs and endogenous siRNAs in *C. elegans*. Cell. **127,** 1193–1207.

Schnepf, E., and Reinhard, C. (1997). Brachycytes in *Funaria* protonemate: induction by abscisic acid and fine structure. Plant Physiol. **151,** 166–175.

Strepp, R., Scholz, S., Kruse, S., Speth, V., and Reski, R. (1998). Plant nuclear gene knockout reveals a role in plastid division for the homolog of the bacterial cell division protein FtsZ, an ancestral tubulin. Proc. Natl Acad. Sci. U S A. **95,** 4368–4373.

Talmor-Neiman, M., Stav, R., Klipcan, L., Buxdorf, K., Baulcombe, D.C., and Arazi, T. (2006). Identification of *trans*-acting siRNAs in moss and an RNA-dependent RNA polymerase required for their biogenesis. Plant J. **48,** 511–521.

Tamura, K., and Nei, M. (1993). Estimation of the number of nucleotide substitutions in the control region of mitochondrial DNA in humans and chimpanzees. Mol. Biol. Evol. **10,** 512–526.

Tamura, K., Peterson, D., Peterson, N., Stecher, G., Nei, M., and Kumar, S. (2011). MEGA5: molecular evolutionary genetics analysis using maximum likelihood, evolutionary distance, and maximum parsimony methods. Mol. Biol. Evol. **28,** 2731–2739.

Vandenbussche, F., Fierro, A.C., Wiedemann, G., Reski, R., and Van Der Straeten, D. (2007). Evolutionary conservation of plant gibberellin signalling pathway components. BMC Plant Biol. **7,** 65.

Vaucheret, H. (2006). Post-transcriptional small RNA pathways in plants: mechanisms and regulations. Genes Dev. **20,** 759–771.

Vazquez, F. (2006). *Arabidopsis* endogenous small RNAs: highways and byways. Trends Plant Sci. **11,** 460–468.

Vazquez, F., et al. (2004). Endogenous *trans*-acting siRNAs regulate the accumulation of *Arabidopsis* mRNAs. Mol. Cell. **16,** 69–79.

Wu, G., and Poethig, R.S. (2006). Temporal regulation of shoot development in *Arabidopsis thaliana* by miR156 and its target SPL3. Development. **133,** 3539–3547.

Wu, G., Park, M.Y., Conway, S.R., Wang, J.W., Weigel, D., and Poethig, R.S. (2009). The sequential action of miR156 and miR172 regulates developmental timing in *Arabidopsis*. Cell. **138,** 750–759.

Xie, Z., Allen, E., Wilken, A., and Carrington, J.C. (2005). DICER-LIKE 4 functions in *trans*-acting small interfering RNA biogenesis and vegetative phase change in *Arabidopsis thaliana*. Proc. Natl Acad. Sci. U S A. **102,** 12984–12989.

Xie, Z., et al. (2004). Genetic and functional diversification of small RNA pathways in plants. PLoS Biol. **2,** E104.

Yoshikawa, M., Peragine, A., Park, M.Y., and Poethig, R.S. (2005). A pathway for the biogenesis of *trans*-acting siRNAs in *Arabidopsis*. Genes Dev. **19,** 2164–2175.

Zemach, A., McDaniel, I.E., Silva, P., and Zilberman, D. (2010). Genome-wide evolutionary analysis of eukaryotic DNA methylation. Science. **328,** 916–919.